physica status solidi rrl
www.pss-rapid.com

Chemical Stability of IrO_2 Top Electrodes in Ferroelectric $Hf_{0.5}Zr_{0.5}O_2$-Based Metal–Insulator–Metal Structures: The Impact of Annealing Gas

*Thomas Szyjka, Lutz Baumgarten, Terence Mittmann, Yury Matveyev, Christoph Schlueter, Thomas Mikolajick, Uwe Schroeder, and Martina Müller**

The IrO_2 top electrode chemistry of ferroelectric $IrO_2/Hf_{0.5}Zr_{0.5}O_2$ (HZO)/IrO_2 metal–insulator–metal (MIM) structures dependent on rapid thermal annealing in different gas atmospheres (nitrogen, oxygen, and forming gas [FG]) is investigated. Using hard X-ray photoelectron spectroscopy (HAXPES), the strongly modified chemical states of the IrO_2 layer dependent on the choice of annealing gas atmosphere are observed. For O_2 and N_2 anneals, the IrO_2 electrode remains either unaffected or is just slightly chemically attacked at the top. In contrast, FG annealing causes a complete reduction of the IrO_2 top electrode into metallic Ir. Surprisingly, oxygen is detected—unbound to Ir—which is incorporated in the metallic Ir layer. This mobile oxygen is thought to affect the electrical behavior of the IrO_2/HZO/IrO_2 device. In addition, it may serve as a test sample for future studies of the root causes of the role of oxygen-vacancy interactions at the interface, which can influence the performance instabilities in HZO-based MIM structures, such as wake-up, imprint, and fatigue.

1. Introduction

Ferroelectric memory devices are envisioned for future next-generation non-volatile memory applications,[1] whereby the proposed active ferroelectric layer has changed from perovskite to HfO_2-based oxide layers due to its better complementary metal–oxide–semiconductor compatibility.[2,3] It has been shown that amorphous HfO_2 can be crystallized into a ferroelectric phase by suitable doping and annealing conditions.[4,5] Moreover, an equal mixture of HfO_2 and ZrO_2 is widely used due to its low crystallization temperature and higher polarization value.[6,7] The electrical performance of $Hf_{0.5}Zr_{0.5}O_2$ (HZO)-based ferroelectric devices is strongly governed by the presence of oxygen vacancies, which, in turn, stabilize the ferroelectric orthorhombic phase. Moreover, it is well known that in metal–insulator–metal (MIM) capacitors, the choice of particular electrode materials and the resulting interfaces to the ferroelectric layer are of utmost relevance for their performance,[8] in particular determining the defect-related mechanisms, such as wake-up, imprint, and fatigue.[3]

As an oxide electrode material, IrO_2 used as top and bottom electrodes has already been shown to increase the ferroelectric performance of the perovskite material $Pb(Zr_xTi_{1-x})O_3$ (PZT).[9,10] This effect was attributed to the annihilation of vacancies by an additional oxygen supply from the IrO_2 electrodes. Therefore, the application of IrO_2 as an alternative electrode material in HZO-based MIM structures is considered promising.

To transform an as-deposited, amorphous HZO interlayer into its ferroelectric orthorhombic phase, a crystallization process is applied after deposition. This is accomplished by a rapid thermal annealing (RTA) step, and the choice of the appropriate annealing atmosphere is essential to either avoid or induce subsequent chemical reactions in the respective MIM layers. Nitrogen annealing (NA) is typically used to avoid chemical reactions due to its inert character, whereas an oxygen annealing (OA) atmosphere can improve the oxidation state of unstable oxides or not completely oxidized layers.[11] Forming gas annealing (FGA) is essential for silicon-based devices. To enable an integration of ferroelectric MIM structures, an FGA treatment would be necessary. This, however, is known

T. Szyjka, Dr. L. Baumgarten
Forschungszentrum Jülich GmbH
Peter Grünberg Institut (PGI-6)
Jülich 52425, Germany

T. Mittmann, Prof. T. Mikolajick, Dr. U. Schroeder
NaMLab gGmbH
Noethnitzer Str. 64a, Dresden 01187, Germany

Dr. Y. Matveyev, Dr. C. Schlueter
Deutsches Elektronen-Synchrotron
Notkestrase 85, Hamburg 22607, Germany

Prof. T. Mikolajick
Chair of Nanoelectronics
TU Dresden
Dresden 01062, Germany

Prof. M. Müller
Fachbereich Physik
Universität Konstanz
Konstanz 78457, Germany
E-mail: martina.mueller@uni-konstanz.de

The ORCID identification number(s) for the author(s) of this article can be found under https://doi.org/10.1002/pssr.202100027.

DOI: 10.1002/pssr.202100027

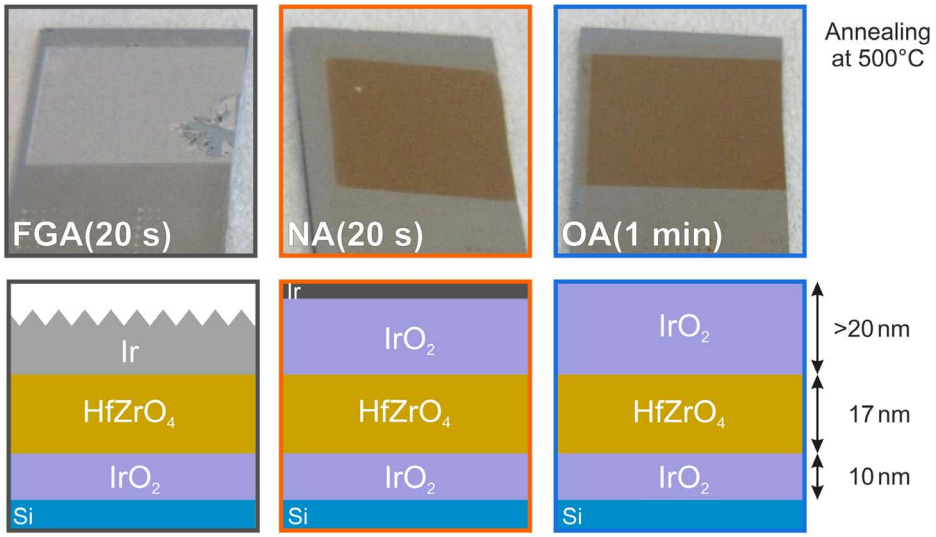

Figure 1. (Top) Pictures of IrO_2/HZO/IrO_2 samples after RTA in different gas atmospheres (FG, N_2, and O_2). Optical inspections already reveal significant chemical modifications of the IrO_2 top electrode. HAXPES data reveal the chemical state of the respective samples. (Bottom) Schematics of the ferroelectric IrO_2/HZO/IrO_2 MIM structures after RTA.

to be decremental to perovskite and layered perovskite ferroelectrics.[12]

To retrace chemical modifications that are directly related to these different RTA crystallization processes, we present an investigation of the local chemistry of top electrode in IrO_2/HZO/IrO_2 MIM structures. We investigate the chemical state of the top IrO_2 electrode dependent on the RTA atmosphere, i.e., anneals in NA, OA, and FGA atmosphere, as schematically shown in **Figure 1**. Hard X-ray photoelectron spectroscopy (HAXPES) is used as an element- and depth-sensitive characterization technique.[13–15] Its information depth enables an investigation of the entire top electrode and the underlying HZO. In the way, we collect clear pictures of the chemical modifications of IrO_2 electrodes due to the RTA of IrO_2/HZO/IrO_2 MIM structures. In this study, we primarily focus on the local chemistry of the top electrode and further discuss the possible implications on the defect structure of the ferroelectric HZO layer. The results may stimulate further investigations and finally aid to a better understanding and control of performance instabilities, such as wake-up, imprint, and fatigue.[16]

2. Results and Discussion

In **Figure 2**a, spectral overview from the Fermi level up to a binding energy (E_B) of 80 eV is displayed for all samples annealed in N_2, O_2, or FG. The prominent Ir 4f and Ir 5p core levels located between $E_B = 45$ and 70 eV show a significant difference in peak shape and binding energy: The spectrum of the FGA sample is shifted by about 800 meV to lower binding energies compared with the NA and OA samples. Whereas the NA and OA spectra reveal the typical peak shape and binding energy position expected for IrO_2, the FGA spectrum is a clear fingerprint for purely metallic iridium (Ir). A closer investigation of the NA and OA Ir 4f core levels also reveals a small component of

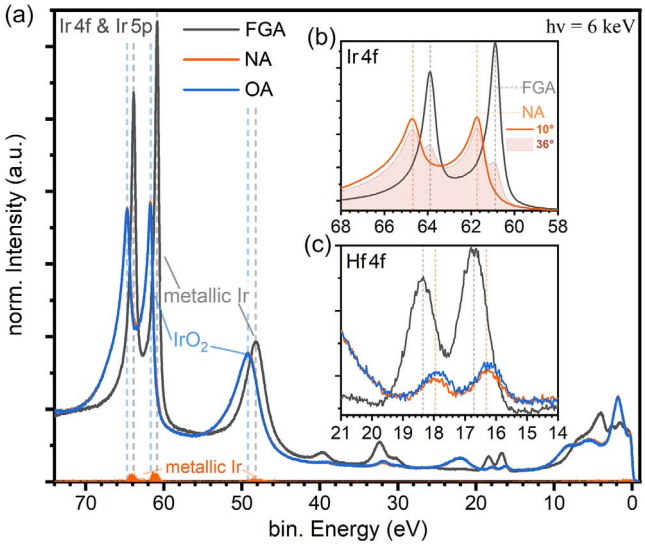

Figure 2. a) HAXPES overview spectra of the FGA, NA, and OA samples, ranging from the Ir 4f and Ir 5p core level up to E_F, including the Hf 4f core level. All spectra are normalized to the integrated signal of the Ir core levels. To work out the differences between NA and OA, the NA spectrum was subtracted by the OA one yielding the metallic Ir proportions (see shaded orange area). b) Zoom into the Ir 4f core level of the FGA and NA including an additional surface-sensitive angle measurement (36°) of NA (filled area). c) Expansion of Hf 4f peaks. The binding energy of the Hf 4f peaks of FGA is shifted by 400 meV compared with NA and OA, respectively.

metallic iridium underlying the dominating IrO_2 emission of the NA sample, which was extracted by calculating the difference spectra between NA and OA. A more surface sensitive spectrum recorded at an emission angle of 36° clearly reveals that this metallic component is located on top of the IrO_2 top electrode (see inset of Figure 2b). An estimate of the thickness results

in a coverage of one monolayer or less. These results are in full agreement with recent results published by Heikkilä et al.,[17] who found IrO_2 thin films being chemically stable up to the annealing temperatures of 1000 °C in oxygen atmosphere, whereas IrO_2 decomposes into metallic Ir for annealing in N_2 atmosphere above 500 °C. For annealing in vacuum or in FG, the reduction already starts at 250 °C.

Moving on to the Hf-related emission features located between 15 and 20 eV in Figure 2, these Hf 4f core levels show a rigid binding energy shift of 400 meV for the FGA sample compared with the NA and OA (see inset of Figure 2c), and the FGA sample also reveals a significant increase in spectral intensity. However, the Hf 4f peak shapes are similar to the NA, OA, and FGA samples, respectively. These observations will be discussed in more detail in the following.

Next, we will discuss the oxygen-related features by means of the O 1s peak, as shown in **Figure 3**. All spectra are normalized to the same Ir 4f intensity of the top electrode. As expected from the previous findings on Ir 4f, and Ir 5p, the NA and OA spectra display a strong O 1s emission originating from the IrO_2 top electrode, which is absent for the FGA sample due to its complete reduction into metallic Ir. For the FGA sample, the result for an additional angle is plotted. In normal emission geometry (more bulk sensitive), the FGA spectrum shows two components at 530.5 and 533.7 eV binding energy. The lower binding energy feature at 530.5 eV, which coincides with the IrO_2 component of the NA and OA samples, is identified with the oxygen emission originating from HZO. This component decreases for the more surface sensitive spectrum taken at 41°, as expected for an HZO emission located below the top electrode. The O 1s peak intensity at 533.7 eV shows the same tendency as the Ir 4f top electrode emission. Thus, due to the normalization to the Ir 4f top electrode emission, its intensity does not change upon the emission angle.

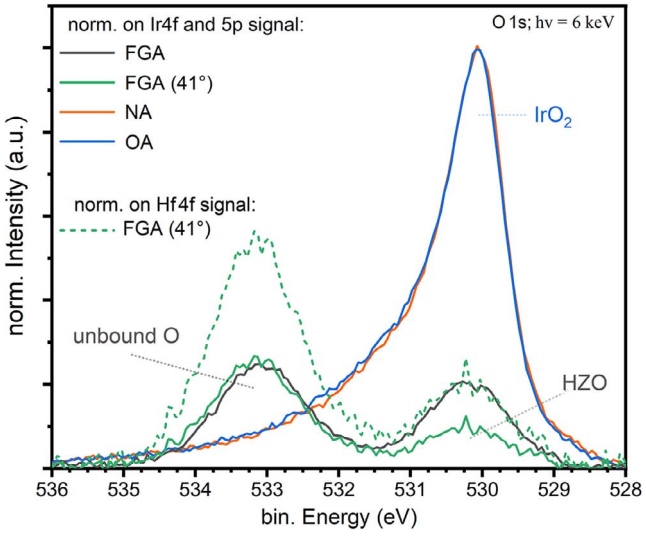

Figure 3. HAXPES O 1s spectra of the FGA, NA, and OA samples. In addition, a surface-sensitive measurement of FGA is shown (green line). The spectra are normalized to the integrated signal of the Ir 4f and Ir 5p core levels. In addition, the surface-sensitive measurement of FGA is also plotted normalized to the Hf 4f signal.

Thus, it should be related to an oxygen component within the metallic iridium top layer. It should be noted that there is no signature of IrO_2 in the FGA-annealed Ir 4f spectrum within the experimental HAXPES sensitivity. Time of flight secondary ion mass spectroscopy data with its higher elemental sensitivity, however, suggest a small IrO_2 component at the interface of the same samples.[16]

We now discuss the influence of the different annealing processes of the IrO_2 top electrode on the HZO layer. In **Figure 4**b, we show the Hf 4f spectra of a reference sample without top electrode, which obviously are not impacted by the respective annealing atmosphere, neither in peak shape nor in binding energy. In Figure 4a, the Hf 4f spectra for the samples annealed with top electrode are shown. The NA and OA spectra do not differ in shape or intensity, but they reveal a small binding energy shift of ≈200 meV compared with the sample without top electrode shown in Figure 4b. The FGA spectrum shows a shift of 400 meV compared with the NA and OA spectra. No apparent differences can be observed in the peak shapes, although a detailed comparison is hindered by the low statistics caused by the damping through the 20 nm IrO_2 thick top electrode.

In summary, we find that the NA and OA samples spectroscopically behave mostly identical, because only small differences are evident from the IrO_2 top electrode and the HZO active layer core-level signatures. This observation is also backed by our electrical measurements shown in **Figure 5**, in which we found almost similar pristine polarization values for the NA and OA samples while the subsequent field cycling behavior differs.[16]

In contrast, the FGA sample shows several and significant chemical modifications, which likely affects the MIM capacitor structure. We resume the three major observations: The first and most obvious one, evident even by optical inspection (see Figure 1) and confirmed by HAXPES, is the complete reduction of the IrO_2 top electrode to metallic iridium. Second, we detect oxygen contributions in the metallic Ir top electrode—but

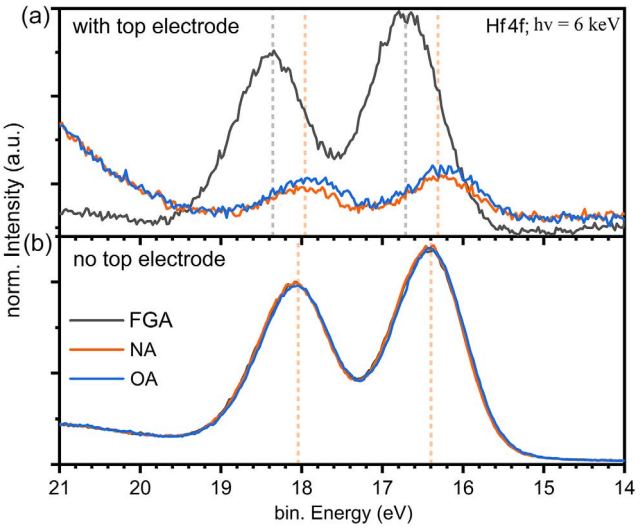

Figure 4. a,b) HAXPES Hf 4f spectra of FGA, NA, and OA samples with (a) and without (b) top electrode. In (a), a binding energy shift of 400 meV between the spectra of FGA and the other samples is apparent. The Hf 4f peaks in (b) have the same binding energy.

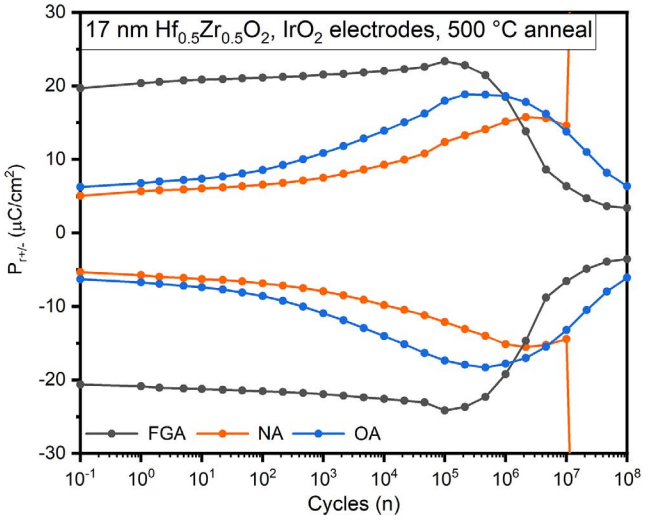

Figure 5. Ferroelectric polarization versus switching cycles of FG (9:1 N_2:H_2 ratio)-, N_2-, and O_2-annealed samples (see also Mittmann et al.[16]).

present as species unbound to Ir, as revealed by the O 1s spectrum. Third, the electrostatic properties of the HZO layer are affected by FGA, apparent by a rigid binding energy shift (≈400 meV) of all HZO-related core levels compared with those of the NA and OA samples. Hence, we will discuss the impact of FG annealing—particularly regarding the modified chemical state of the IrO_2 top electrode and the possibly altered MIM capacitor in more detail.

As a consequence of our first observation, the reduction of the IrO_2 top electrode to metallic iridium caused by the FGA should be accompanied by a change of the volume, i.e., the thickness of the top electrode: The fcc Ir metal lattice cell contains four Ir atoms within a volume of roughly 57 $Å^3$, whereas, in an IrO_2 unit cell, four Ir atoms are distributed in a volume of about 128 $Å^3$. Assuming mass conservation, the removal of oxygen from IrO_2 should result in a reduced volume and, thus, in a reduced film thickness, which is indeed observed by HAXPES: The intensity of the underlying HZO signal increases compared with the NA and OA samples. An effective film thickness can be estimated by comparing the Hf 4f intensities at 10° and 41° emission angle. Using the density and mean free path of Ir bulk metal, this "effective" Ir top layer thickness is estimated as ≈9 nm. Even though the Ir 4f spectrum shows a purely metallic shape, the morphology of the reduced Ir top electrode most likely is far from a flat and smooth metal film, because also a lateral reduction of the film dimension must be considered. The relaxation of lateral stress can also result in a macroscopic damage of the film, which is evident in Figure 1, e.g., at the lower right-hand side of the FGA sample. Therefore, the calculated film thickness should be taken as an estimated lower limit of the layer thickness. A concomitant roughening of the FGA sample surface is, in fact, observed by scanning electron microscopy.[16]

Taking up the second observation, the presence of oxygen unbound to Ir within the metallic Ir top layer seems to be astonishing, at least at first glance. At second glance, Ir is a noble-like metal, and its oxidation is thermodynamically unfavorable, which results, for example, in the rather large instability of IrO_2 upon annealing.

Beyond the well-known fact that IrO_2 readily decomposes during annealing in nitrogen, FG, or even in vacuum,[17–19] more detailed investigations on the reduction process itself are rare in the literature. Shan et al. investigated the fragmentation of IrO_2 nanotubes upon annealing in vacuum.[20] They observed a complete reduction to metallic iridium upon annealing temperatures up to 600 °C. The morphology of the remaining metallic Ir nanotubes was highly porous and contained unbound oxygen, revealed by an O 1s photoemission at a binding energy of 532.4 eV. On the other hand, the reverse process of Ir oxidation was investigated by Novotny et al.[21] They observed subsurface incorporation of oxygen as a precursor of the complete IrO_2 formation, which was reflected by the appearance of an O 1s peak at 531.8 eV. In both investigations, the incorporation of unbound oxygen species into the metallic Ir was observed, which is in agreement with our HAXPES results for the FGA sample. Although this oxygen is definitely unbound to Ir, its chemical state requires further investigation. From the observed binding energy position, its origin may be attributed either to hydroxyl groups or water. We note that the appearance of this oxygen within the metallic Ir top layer might be of significant importance for the performance of the ferroelectric device. It may serve as an oxide reservoir to fill up oxide defects in HZO at the interface and, in this way, may enable a more controlled oxygen vacancy density diffusion under electrical field cycling.

Discussing finally the third observation, we compare our results to a recent work by Hyuk Park et al.,[22] who investigated the impact of FG annealing on a ferroelectric HZO layer—but with Pt top electrodes. They found degradation of the ferroelectric properties for FGA at the annealing temperatures below 500 °C. A partial recovery of the ferroelectric polarization is observed for higher annealing temperatures, but its value is always below the polarization of a N_2-annealed sample. The corresponding X-ray photoelectron spectroscopy (XPS) spectra showed a rigid shift of the HZO-related spectra. FGA on HZO without top electrode does not show any shift.

These XPS results for a Pt top electrode are in general agreement with our HAXPES results for the IrO_2 top electrode reduced to metallic Ir. Without top electrode, FGA has no effect on the binding energy of the HZO-related spectra such as Hf 4f and Zr 3d, in comparison with NA and OA samples. With top electrode, the Hf 4f spectrum shows a shift of 400 meV toward higher binding energies after FGA. Hyuk Park et al. proposed the metallic Pt top electrode to act as a catalyst for hydrogen incorporation in HZO,[22] which was already observed before for PZT and $SrBi_2Ta_2O_9$.[23–25] As Pt and Ir are chemically very similar, we may assume that this catalytic effect likely occurs in Ir as well.

The impact of H incorporation on the HZO layer is contrary; however, the ferroelectric polarization deteriorates upon FGA compared to NA with Pt top electrode in Hyuk Park's study. In our study, the polarization increases for FGA compared to NA with Ir top electrode (see Figure 5). A significant difference between our study and the work by Hyuk Park et al.[22] is that the Pt electrode was deposited as a thin film, whereas the metallic Ir top electrode is a result of the reduction of IrO_2 during FGA. Hence, we may assume that this chemical modification also has a direct impact on the HZO layer.

Due to its large electronegativity, hydrogen atoms can act as an electron donor or electron capture, particularly for vacancy electrons. In case of vacancy electron capturing, the vacancy gap states should be electronically passivated[26] and result in a shift of the Fermi level. In a previous study, we have revealed such a process by the incorporation of nitrogen in HfO_2.[27] As vacancy gap states are mainly expected near the conduction band minimum (CBM),[26,28] such passivation should result in a Fermi level shift toward the valence band maximum (VBM), and, in accordance, a rigid core-level shift toward lower binding energies was observed for nitrogen incorporation.[27] In the present study, we do not observe a core-level shift for FGA samples toward lower binding energies, but, in contrary, toward higher ones and, hence, conclude that hydrogen does not passivate existing defect states in HZO but introduces additional ones.

3. Conclusion

We present an HAXPES study of ferroelectric IrO_2/HZO/IrO_2 MIM structures and focus, in particular, on the IrO_2 top electrode chemistry dependent on thermal annealing in different gas atmospheres (nitrogen, oxygen, and FG). We primarily observe very different thermal stabilities of the IrO_2 layer dependent on the choice of annealing gas atmosphere: The IrO_2 electrode remains chemically stable for annealing in oxygen atmosphere. For annealing in nitrogen atmosphere, a chemical reduction of the IrO_2 electrode starts and results in metallic Ir layer on top of the IrO_2 electrode. Finally, FGA causes a complete reduction of the IrO_2 top electrode into metallic Ir. Especially notable is that this metallic Ir layer contains oxygen, unbound to Ir, which is expected to affect the underlaying HZO and modify its defect structure, e.g., during electric field cycling. In contrast, the ferroelectric HZO layer should remain mostly unaffected for nitrogen and oxygen anneals, and no strong chemically induced modification of its defect structure is expected.

The results yield a clear picture of the chemical modifications of IrO_2 electrodes during the crystallization step of IrO_2/HZO/IrO_2 MIM structures. Moreover, different possible implications on the defect structure of the ferroelectric HZO layer are discerned. In particular, the FG-annealed IrO_2 top electrode with its unbound oxygen content may serve as a test system for further studies on electric-field-driven interactions between oxygen containing electrodes and vacancies within the ferroelectric layer. This may aid to a better understanding and control of performance instabilities such as wake-up, imprint, and fatigue.

4. Experimental Section

The IrO_2/HZO/IrO_2 sample stack was grown on a boron-doped Si substrate. The nominal 10 nm IrO_2 bottom and 17–20 nm top electrodes were deposited by sputtering from a pure Ir target with a process gas of a 20:5 sccm Ar:O_2 ratio at a pressure of 0.1 Pa and a power of 25 W. The 17 nm thick HZO film was grown by atomic layer deposition (ALD) at 250 °C substrate temperature with 75 supercycles of Hf[N(CH3)(C2H5)]4 and CpZr[N(CH3)2]3 precursors as Hf and Zr sources. Oxygen plasma was used as an oxidant. The IrO_2 top electrodes were sputtered through a shadow mask with an array of dots with diameters ranging from 110 to 450 µm and an additional rectangular window of ≈1 cm^2 for structural X-ray characterization. Further experimental details on sample preparation and characterization are published by Materano et al.[7] and Mittmann et al.[16] This sample is split into three parts to undergo a different crystallization anneal step for each sample. Thus, all samples were equivalent until the crystallization anneal step. Annealing was made in a rapid thermal processing tool in nitrogen, oxygen, or FG ambient (9:1 N_2:H_2 ratio); 500 °C as annealing temperature was used, because IrO_2 is thermally instable.

HAXPES was performed at the P22 beamline of PETRA III (DESY, Hamburg)[29] to investigate depth-dependent chemical properties. The data allow us to conclude on the chemical properties and possible interactions of the HZO_2 layer and the top electrode interface.[13] Core-level spectra of Hf, Zr, Ir, and O were recorded at a photon energy of 6 keV. HAXPES, thereby, provides the large information depth required to probe the entire capacitor stack;[15,30] even signals from the IrO_2 bottom electrode could be detected.[16] For a depth-dependent analysis, we recorded HAXPES spectra at the photoelectron emission angles of 10° (more bulk sensitive) as well as for 36° and 41° (more surface sensitive) relative to the surface normal. Binding energies (E_B) are referred to the Fermi level of gold.

Acknowledgements

This project has received funding from the European Union's Horizon 2020 research and innovation programme under grant agreement No. 780302. The authors acknowledge DESY (Hamburg, Germany), a member of the Helmholtz Association HGF, for the provision of experimental facilities. Funding for the HAXPES instrument at beamline P22 by the Federal Ministry of Education and Research (BMBF) under contracts 05KS7UM1 and 05K10UMA with Universität Mainz and 05KS7WW3, 05K10WW1, and 05K13WW1 with Universität Würzburg is gratefully acknowledged.

Open access funding enabled and organized by Projekt DEAL.

Conflict of Interest

The authors declare no conflict of interest.

Data Availability Statement

Research data are not shared.

Keywords

ferroelectric $Hf_{0.5}Zr_{0.5}O_2$, IrO_2, metal–insulator–metal structures, rapid thermal annealing, top electrode chemistry

Received: January 14, 2021
Revised: February 11, 2021
Published online: March 17, 2021

[1] H. Kohlstedt, Y. Mustafa, A. Gerber, A. Petraru, M. Fitsilis, R. Meyer, U. Böttger, R. Waser, *Microelectron. Eng.* **2005**, *80*, 296.
[2] F. P. G. Fengler, M. Pešic, S. Starschich, T. Schneller, U. Böttger, T. Schenk, M. H. Park, T. Mikolajick, U. Schroeder, in *2016 46th European Solid-State Device Research Conf. (ESSDERC)*, IEEE, Piscataway, NJ, USA **2016**, pp. 369–372; https://doi.org/10.1109/ESSDERC.2016.7599663.
[3] M. H. Park, Y. H. Lee, T. Mikolajick, U. Schroeder, C. S. Hwang, *MRS Commun.* **2018**, *8*, 795.
[4] T. S. Böscke, J. Müller, D. Bräuhaus, U. Schröder, U. Böttger, *Appl. Phys. Lett.* **2011**, *99*, 102903.
[5] T. Mittmann, M. Materano, P. D. Lomenzo, M. H. Park, I. Stolichnov, M. Cavalieri, C. Zhou, C.-C. Chung, J. L. Jones, T. Szyjka, M. Müller,

A. Kersch, T. Mikolajick, U. Schroeder, *Adv. Mater. Interfaces* **2019**, *6*, 1900042.
[6] J. Müller, T. S. Böscke, D. Bräuhaus, U. Schröder, U. Böttger, J. Sundqvist, P. Kücher, T. Mikolajick, L. Frey, *Appl. Phys. Lett.* **2011**, *99*, 112901.
[7] M. Materano, C. Richter, T. Mikolajick, U. Schroeder, *J. Vac. Sci. Technol. A* **2020**, *38*, 022402.
[8] T. Szyjka, L. Baumgarten, T. Mittmann, Y. Matveyev, C. Schlueter, T. Mikolajick, U. Schroeder, M. Müller, *ACS Appl. Electron. Mater.* **2020**, *2*, 3152.
[9] H. Fujisawa, S. Hyodo, K. Jitsui, M. Shimizu, H. Niu, H. Okino, T. Shiosaki, *Integr. Ferroelectr.* **1998**, *21*, 107.
[10] T. Nakamura, Y. Nakao, A. Kamisawa, H. Takasu, *Jpn. J. Appl. Phys.* **1994**, *33*, 5207.
[11] M. H. Hamed, D. N. Mueller, M. Müller, *J. Mater. Chem. C* **2020**, *8*, 1335.
[12] W. Hartner, G. Schindler, P. Bosk, Z. Gabric, M. Kastner, G. Beitel, T. Mikolajick, C. Dehm, C. Mazuré, *Integr. Ferroelectr.* **2000**, *31*, 273.
[13] M. Müller, S. Nemšák, L. Plucinski, C. M. Schneider, *J. Electron Spectrosc. Related Phenom.* **2016**, *208*, 24.
[14] T. Gerber, P. Lömker, B. Zijlstra, C. Besson, D. N. Mueller, W. Zander, J. Schubert, M. Gorgoi, M. Müller, *J. Mater. Chem. C* **2016**, *4*, 1813.
[15] C. Caspers, A. Gloskovskii, M. Gorgoi, C. Besson, M. Luysberg, K. Rushchanskii, M. Ležaic, C. S. Fadley, W. Drube, M. Müller, *Sci. Rep.* **2016**, *6*, 22912.
[16] T. Mittmann, T. Szyjka, L. Baumgarten, H. A. Hsain, M. C. Istrate, P. D. Lomenzo, I. Karpov, M. Müller, J. L. Jones, L. Pintille, T. Nicolajick, U. Schröder, *Phys. Status Solidi* https://doi.org/10.1002/pssr.202100012.
[17] M. J. Heikkilä, J. Hämäläinen, E. Puukilainen, M. Leskelä, M. Ritala, *J. Appl. Crystall.* **2020**, *53*, 369.
[18] T.-S. Chen, V. Balu, B. Jiang, S.-H. Kuah, J. C. Lee, P. Chu, R. E. Jones, P. Zurcher, D. J. Taylor, S. Gillespie, *Integr. Ferroelectr.* **1997**, *16*, 191.
[19] J. S. Cross, Y. Horii, N. Mizuta, S. Watanabe, T. Eshita, *Jpn. J. Appl. Phys.* **2002**, *41*, 698.
[20] C.-C. Shan, D.-S. Tsai, Y.-S. Huang, S.-H. Jian, C.-L. Cheng, *Chem. Mater.* **2007**, *19*, 424.
[21] Z. Novotny, B. Tobler, L. Artiglia, M. Fischer, M. Schreck, J. Raabe, J. Osterwalder, *J. Phys. Chem. Lett.* **2020**, *11*, 3601.
[22] M. Hyuk Park, H. Joon Kim, Y. Jin Kim, W. Lee, H. Kyeom Kim, C. Seong Hwang, *Appl. Phys. Lett.* **2013**, *102*, 112914.
[23] S. Aggarwal, S. R. Perusse, C. W. Tipton, R. Ramesh, H. D. Drew, T. Venkatesan, D. B. Romero, V. B. Podobedov, A. Weber, *Appl. Phys. Lett.* **1998**, *73*, 1973.
[24] Y. Shimamoto, K. Kushida-Abdelghafar, H. Miki, Y. Fujisaki, *Appl. Phys. Lett.* **1997**, *70*, 3096.
[25] J.-P. Han, T. P. Ma, *Appl. Phys. Lett.* **1997**, *71*, 1267.
[26] K. Xiong, J. Robertson, S. J. Clark, *J. Appl. Phys.* **2006**, *99*, 044105.
[27] L. Baumgarten, T. Szyjka, T. Mittmann, M. Materano, Y. Matveyev, C. Schlueter, T. Mikolajick, U. Schroeder, M. Müller, *Appl. Phys. Lett.* **2021**, *118*, 032903.
[28] N. Umezawa, K. Shiraishi, Y. Akasaka, A. Oshiyama, S. Inumiya, S. Miyazaki, K. Ohmori, T. Chikyow, T. Ohno, K. Yamabe, Y. Nara, K. Yamada, *Phys. Rev. B* **2008**, *77*, 165130.
[29] C. Schlueter, A. Gloskovskii, K. Ederer, I. Schostak, S. Piec, I. Sarkar, Y. Matveyev, P. Lömker, M. Sing, R. Claessen, C. Wiemann, C. M. Schneider, K. Medjanik, G. Schönhense, P. Amann, A. Nilsson, W. Drube, S. Gwo, D.-J. Huang, D.-H. Wei, *AIP Conf. Proc.* **2019**, *2054*, 040010.
[30] M. H. Hamed, R. A. Hinz, P. Lömker, M. Wilhelm, A. Gloskovskii, P. Bencok, C. Schmitz-Antoniak, H. Elnaggar, C. M. Schneider, M. Müller, *ACS Appl. Mater. Interfaces* **2019**, *11*, 7576.